Astron. Astrophys. 351, 323–329 (1999)

ASTRONOMY
AND
ASTROPHYSICS

ORFEUS II echelle spectra: On the H_2/CO ratio in LMC gas towards LH 10

P. Richter[1], K.S. de Boer[1], D.J. Bomans[2], Y.-N. Chin[3,4], A. Heithausen[4], and J. Koornneef[5]

[1] Sternwarte, Universität Bonn, Auf dem Hügel 71, 53121 Bonn, Germany
[2] Astronomisches Institut, Ruhr-Universität Bochum, Postfach 102148, 44780 Bochum, Germany
[3] Institute of Astronomy and Astrophysics, Academia Sinica, P.O.Box 1–87, Nankang, 11529 Taipei, Taiwan
[4] Radioastronomisches Institut, Universität Bonn, Auf dem Hügel 71, 53121 Bonn, Germany
[5] Kapteyn Institute, Postbus 800, 9700 AV Groningen, The Netherlands

Received 26 February 1999 / Accepted 19 August 1999

Abstract. *ORFEUS* far UV echelle spectra have been used to investigate H I, H_2 and CO absorption lines along the line of sight towards LH 10:3120 in the LMC, extending the study presented by de Boer et al. (1998). While H_2 absorption is clearly visible, no CO absorption at LMC velocities is detected, but an upper limit of $N(\mathrm{CO}) \leq 3.3 \times 10^{13}\,\mathrm{cm}^{-2}$ for the CO column density is derived for the C-X band near 1088 Å. The detected H_2 absorption features were used to determine a limit for the H_2/CO ratio of $N(H_2)/N(^{12}\mathrm{CO}) \geq 2.0 \times 10^5$ for the LMC gas along this individual line of sight. Generally, the fraction of gas in molecular form in the LMC is low compared to interstellar gas in the Milky Way with the same total gas quantity. We compare the absorption spectroscopy with *SEST* CO emission line measurements. It is found that most of the CO emission comes from gas behind LH 10:3120. We discuss our results in view of the possible scenario, in which the low dust content limits the amount of molecular hydrogen in the diffuse LMC gas.

Key words: space vehicles – stars: individual: LH 10:3120 – ISM: molecules – galaxies: ISM – galaxies: Magellanic Clouds – ultraviolet: ISM

1. Introduction

Molecular hydrogen (H_2) is by far the most abundant molecule in the interstellar medium, followed by carbon monoxide (CO) with a significantly smaller amount. The symmetry of H_2 results in the absence of a permanent dipole moment, which makes the dominant interstellar molecule very difficult to detect. Warm H_2 gas can be observed in near IR emission, but the largest amount of H_2 is located in cold gas, which is measurable in FUV absorption along individual lines of sight against bright UV background sources. Thus the *overall* amount of H_2 in the interstellar medium can not be measured directly. The amount of H_2 often is estimated from the abundance of CO, which can easily be determined from radio emission lines. For this method it is necessary to know the conversion factor X between H_2 column density and the velocity-integrated ^{12}CO emission temperature, defined as $X(^{12}\mathrm{CO}) = N(\mathrm{H_2})/W(^{12}\mathrm{CO})$ (e.g. Heithausen & Mebold 1989).

The X factor has been determined for the Milky Way with some degree of accuracy, using various (indirect) methods (Bloemen et al. 1986). Obviously, it is important to determine the conversion factors in the most nearby lower-metallicity systems (the Magellanic Clouds), too. Cohen et al. (1988) obtained a value which is 6 times as large as in our Galaxy and Rubio et al. (1993) noticed the possible dependence of X on the cloud size. Both results could be affected by the limited angular resolution. Recently, Chin et al. (1997, 1998) estimated the conversion factors in selected regions in the LMC and SMC. A review of molecules and the X factor in the Magellanic Clouds is available from Israel (1997).

An important new aspect for the knowledge of interstellar molecular gas in galaxies with chemical abundances different from those of the Milky Way is the determination of *real* abundance ratios of the H_2 and CO molecules via UV absorption spectroscopy. This is also the most elegant and safe way to decrease the uncertainties in the measurements of the X factor in those systems. The *Copernicus* satellite could measure the relation between H_2 and CO for the diffuse interstellar gas in the Milky Way (Federman et al. 1980). However, every individual H_2/CO ratio definitely is influenced by the metallicity, by the local radiation field and by the amount of dust in the observed complex. So far, H_2/CO ratios from absorption spectroscopy could not be measured outside the Milky Way. The sensitvity of *Copernicus* was not high enough while the *IUE* satellite as well as the *HST* do not cover the wavelength range below 1200 Å, where H_2 is found in absorption. *ORFEUS* is the first instrument able to investigate the cold molecular gas in the Magellanic Clouds via absorption spectroscopy.

Using *ORFEUS* data we measured H_2 absorption profiles toward one LMC (de Boer et al. 1998, hereafter Paper I) and one SMC (Richter et al. 1998) star. Among the observed Magellanic Cloud lines of sight only the one to the star 3120 (Parker et al. 1992) in the association LH 10 in the LMC shows a column densitiy in H_2 high enough to expect the presence of CO.

Send offprint requests to: prichter@astro.uni-bonn.de

Table 1. Basic properties of the target star in the LMC

Object	V [mag]	$E(B-V)$ [mag]	Spectral type	l	b
LH 10:3120	12.80	0.17	O5.5 V	277.2	−36.1

The *ORFEUS* spectrum of LH 10:3120 therefore provides the very first opportunity to determine a H_2/CO ratio for LMC gas directly.

2. ORFEUS absorption line measurements

2.1. Instrument description

The spectroscopic data were obtained with the Heidelberg-Tübingen echelle spectrometer during the *ORFEUS II* mission on the *ASTRO-SPAS* space shuttle mission between November and December 1996. *ORFEUS* (Orbiting and Retrievable Far and Extreme Ultraviolet Spectrometer) consists of a 1 m normal incidence mirror with a focal length of 2.4 m. The echelle operated in the diffraction orders 40 to 61 in the wavelength range from 900 to 1400 Å. The echelle spectrometer was designed to achieve a spectral resolution of $\lambda/\Delta\lambda = 10^4$ in an entrance aperture of $10''$ (Appenzeller et al. 1988), but turned out to be more accurate ($\simeq 1.2\times10^4$) during the measurements (Barnstedt et al. 1999). At 1000 Å this value corresponds to a resolution of 83 mÅ or 25 km s^{-1}.

The echelle detector is a photon counting microchannel plate detector with 1024 by 512 pixels in an active area of 44×44 mm. A detailed description of the instrument is given by Barnstedt et al. (1999).

2.2. Observations

The target star for our observation was star 3120, located in the association LH 10 in the north-western part of the LMC in the N 11 superbubble complex (see Paper I). Basic properties of the background star (Parker et al. 1992) have been summarized in Table 1. The star has been observed in 3 pointings with an effective observing time of ~ 6000 s.

2.3. Data reduction

The basic data reduction, such as the correction of the blaze function, the wavelength calibration and the background substraction, has been performed by the *ORFEUS* team in Tübingen. The mean accuracy for the wavelength calibration is ≤ 50 mÅ and thus better than the spectral resolution of the instrument (Barnstedt et al. 1999). Moreover, the wavelength scale has been corrected for the orbital movement of the satellite and the Earth's movement. The background substraction, as described in Barnstedt et al. (1999), has taken into account contributions from the intrinsic background of the detector, from straylight and from particle events related to the South Atlantic Anomaly. For the flux calibration they give an internal accuracy of $\pm10\%$.

Table 2. H_2 equivalent widths for the Lyman band in the LMC gas towards LH 10:3120

Line	λ [Å]	f	W_λ [mÅ]	Error [mÅ]
$J=0$, $g_J=1$, $E_J=0$ eV, $\log N = 18.7\pm0.2$ cm^{-2}				
R(0),0-0	1108.128	0.00173	186	31
R(0),1-0	1092.194	0.00596	244	40
$J=1$, $g_J=9$, $E_J=0.01469$ eV, $\log N = 18.1\pm0.1$ cm^{-2}				
R(1),0-0	1108.634	0.00117	104	23
R(1),1-0	1092.732	0.00403	154	25
R(1),2-0	1077.698	0.00809	191	39
P(1),2-0	1078.925	0.00385	137	32
P(1),4-0	1051.031	0.00403	154	25
$J=2$, $g_J=5$, $E_J=0.04394$ eV, $\log N = 17.7\pm0.2$ cm^{-2}				
R(2),0-0	1110.120	0.00107	108	25
R(2),2-0	1079.226	0.00739	124	28
R(2),5-0	1038.690	0.01700	155	33
$J=3$, $g_J=21$, $E_J=0.08747$ eV, $\log N = 17.5\pm0.4$ cm^{-2}				
R(3),4-0	1053.976	0.01420	123	26
R(3),5-0	1041.156	0.01640	139	32
P(3),5-0	1043.498	0.01040	129	28
$J=4$, $g_J=9$, $E_J=0.14491$ eV, $\log N = 16.7\pm0.4$ cm^{-2}				
R(4),2-0	1085.144	0.00700	94	31
P(4),2-0	1088.794	0.00487	83	25
P(4),4-0	1060.580	0.00930	87	28
Total H_2: $\log N = 18.8\pm0.2$ cm^{-2}				

Because of the low count rate in the spectrum of LH 10:3120 the data has been filtered by a de-noising algorithm based on the powerful wavelet transformation, as described by Fligge & Solanki (1997). In principle, the noise in the data is consistent with that expected from photon statistics. The de-noising procedure increases the signal-to-noise ratio (S/N) by a factor of $\sim\sqrt{3}$, at the cost of a slight decrease in the spectral resolution. However, since the target was well centered within the diaphragm, the intrinsic spectral resolution is better than 10^4 (see Sect. 2.1). With respect to the pixel size the resulting spectral resolution after filtering turned out to be ~ 30 km s^{-1}.

2.4. H_2 equivalent width measurements

More than 100 H_2 transitions from the Lyman and Werner bands are located in the wavelength range between 915 and 1140 Å. For the further analysis we took wavelengths and oscillator strengths from the list of Morton & Dinerstein (1976). In general, the strongest H_2 lines are located in the range below 1000 Å. Unfortunately, this is the part of the spectrum where the decreasing sensitivity of the instrument as well as the increasing UV extinction leads to extremely low countrates, so that we had to exclude this wavlength range from the further analysis. Another problem is that the large number of transitions in combination with the expected complex line-of-sight structure let most of the H_2 lines overlap with other H_2 absorption com-

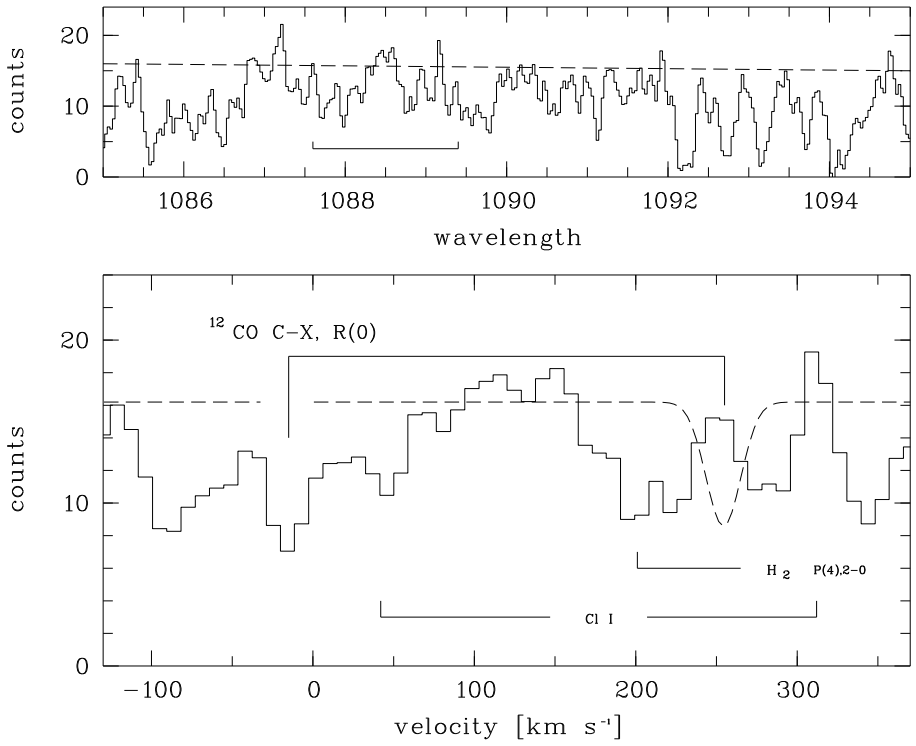

Fig. 1. The spectrum near the ^{12}CO R(0),0-0 line in the C-X band at 1087.87 Å. *Top panel:* The wavelength range between 1085 and 1095 Å plotted in λ-units. The dashed line indicates the adopted continuum level. The marked area is shown enlarged in the the lower panel. *Bottom panel:* The R(0),0-0 line plotted in the velocity scale (LSR). The solid lines indicate the velocties at $-15\,\mathrm{km\,s^{-1}}$ (Milky Way) and $+255\,\mathrm{km\,s^{-1}}$ (LMC). Galactic CO absorption is visible, but no absorption structure is present at the LMC velocity, as indicated by the dashed line showing how a 40 mÅ strong CO line at $+255\,\mathrm{km\,s^{-1}}$ would look like. Other possible absorption structures are identified

ponents. In addition, many atomic transitions, as compiled by Morton (1991), contribute to the confused absorption structure in some parts of the spectrum.

The low S/N ratio does not allow multi-component fits for the absorption features so that decompositions were not possible. Despite these restrictions we found 16 H_2 absorption lines at $v_{\rm LSR} = +255\,\mathrm{km\,s^{-1}}$ from the lowest 5 rotational states, essentially free of line blends in the velocity range between $+220$ and $+300\,\mathrm{km\,s^{-1}}$, for which an analysis of line strengths was possible[1]. For these lines, the equivalent widths were measured by trapezium and (in some cases) by gaussian fits. With respect to the low countrate any more sophisticated method would not lead to a higher accuracy. We measured the equivalent width of each line 3 times independently and used the mean value for the further evaluation.

The formal uncertainties in the equivalent widths are basically due to photon statistics and due to the error for the choice of the continuum. The low count rate and the resulting low S/N ratio causes uncertainties in the determination of the continuum level as well as in the analysis of the line strengths themself. However, the choice of the continuum is in particular critical for weaker absorption structures, but our selection contains basically strong absorption lines. We determined the uncertainty for each line using the following procedure: we fitted (by eye) the continuum around the absorption line and (when necessary) normalized the continuum level. We fitted a maximum and a minimum continuum in order to give an upper and a lower limit for its uncertainty, including the error range for the background substraction. In addition, we obtained the formal uncertainties in the equivalent widths (for a fixed continuum) using the algorithm of Jenkins et al. (1973). The total uncertainty for the equivalent width measurements then was calculated by taking both contributions into account. On the average, the two error sources contribute approximately equal to the total uncertainty.

All H_2 equivalent widths and their errors have been compiled in Table 2. Examples for absorption line profiles can be found in Paper I.

2.5. H_2 column densities

For the further investigation the equivalent widths were used for a standard curve-of-growth analysis for the LMC gas. We find that the best fit for the curve of growth has a b-value of $5\,\mathrm{km\,s^{-1}}$ (see Paper I). For the lower rotational states the b-value is not critical, since their lines are strong and located near the damping part of the curve of growth. Only for $J = 4$ a different b-value would lead to a significant change in the column density for this state. The individual column densities $N(J)$ derived with this method are presented in Table 2. They range from $N(\mathrm{H_2}) = 5.0 \times 10^{16}\,\mathrm{cm^{-2}}$ for $J = 4$ to $N(\mathrm{H_2}) = 4.5 \times 10^{18}\,\mathrm{cm^{-2}}$ for $J = 0$. Fixing the b-value at $5\,\mathrm{km\,s^{-1}}$ the uncertainty for the individual column densities $N(J)$ has been derived by shifting the data points on the curve of growth within their individual error bars to the largest and smallest possible column density. From these values we then determined a mean deviation to the best fit of $N(J)$, as given in Table 2. Summing over all $N(J)$, we find a total H_2 column density of

[1] We note at this point that the velocities presented in Paper I were labeled (by mistake) as LSR velocties while heliocentric velocities were meant. We here correct to LSR velocities with $v_{\rm LSR} = v_{\rm helioc.} - 15\,\mathrm{km\,s^{-1}}$

$N(\mathrm{H_2})_{\mathrm{total}} = 6.6^{+3.4}_{-2.6} \times 10^{18}\,\mathrm{cm^{-2}}$. The empirical curve of growth for all states is shown in Fig. 2 of Paper I.

2.6. H_2 rotational excitation

The determination and interpretation of the rotational excitation of the H_2 gas has been described in Paper I. For $J = 0, 1$ we find an excitation temperature of ≤ 50 K from a fit of a Boltzmann distribution, representing the kinetic gas temperature. For $J = 2, 3$ and 4 the equivalent Boltzmann temperature is 470 K, most likely indicating moderate UV pumping.

2.7. CO absorption

We investigated the amount of carbon monoxide (CO) in the *ORFEUS* spectrum of LH 10:3120 by looking for absorption in the strongest of the ^{12}CO absorption bands, the C-X band near 1088 Å. Other CO bands in the wavelength range of *ORFEUS*, such as the E-X band near 1076 Å, show blendings at LMC velocities or are too weak in comparison to the C-X band. We used wavelengths and oscillator strengths for the CO transitions from the list of Morton & Noreau (1994). Fig. 1 shows the spectral region of the C-X R(0), 0-0 transition. Due to the low S/N ratio and due to a probable blending from Cl I at 1088.06 Å the absorption structure looks rather complex. Moreover, the H_2 P(4), 2-0 line with its galactic component at 1088.79 Å overlaps the CO absorption in the plotted region, as indicated in Fig. 1. Galactic CO absorption near $-15\,\mathrm{km\,s^{-1}}$ is present[2] but there is definitely no absorption visible at $+255\,\mathrm{km\,s^{-1}}$, where the molecular hydrogen in the LMC gas has its absorption (see Fig. 1) and where possible CO absorption from LMC gas should be visible. Obviously, the amount of CO in the LMC gas is too small to be detectable in the *ORFEUS* spectrum of LH 10:3120. Because of the low count rate noise peaks have equivalent widths comparable with those of real absorption lines. Typical noise features are visible near $+280$ and $+340\,\mathrm{km\,s^{-1}}$.

In the following, we derive an upper limit for the ^{12}CO column density by estimating the detection limit for the C-X band. The dominant amount of the CO populates the two ground states with $J = 0, 1$ (Morton & Noreau 1994). For the C-X band, the transitions from these states, $R(0)$, $R(1)$ and $P(1)$, can not be resolved with the resolution of *ORFEUS*. For a rotational temperature of ∼5 K for the CO molecules (as typically found in molecular gas in the Milky Way), the two lowest rotational states ($J = 0, 1$) are approximately equally populated (Morton & Noreau 1994). Under this assumption we can sum over the individual oscillator strengths f of $R(0)$, $R(1)$ and $P(1)$ and find a total value of $f_{0,1} = 0.235$. Based on the noise present and the resulting continuum uncertainty, we place a detection limit of $\simeq 40$ mÅ in the *ORFEUS* spectrum near 1088 Å using the procedure described in Sect. 2.4. This value fits well with the actual upper limit of the strength of a noise peak, as measured in the selected wavelength range. In Fig. 1 a 40 mÅ strong absorption structure at $+255\,\mathrm{km\,s^{-1}}$ is shown as illustration. We find an upper limit for the CO column density in the LMC gas of $N(\mathrm{CO}) \leq 3.3 \times 10^{13}\,\mathrm{cm^{-2}}$ based on the 40 mÅ detection limit and the curve of growth with $b = 5\,\mathrm{km\,s^{-1}}$. This value is valid under the assumption that the H_2 and the CO are located in the same clouds. In that case, the upper limit in $N(\mathrm{CO})$ for each cloud scales downward linearly with W_λ provided that the used b-value is scaled down by the same factor. For multiple identical clouds the limit for $N(\mathrm{CO})_{\mathrm{total}}$ would be the same as the one derived above.

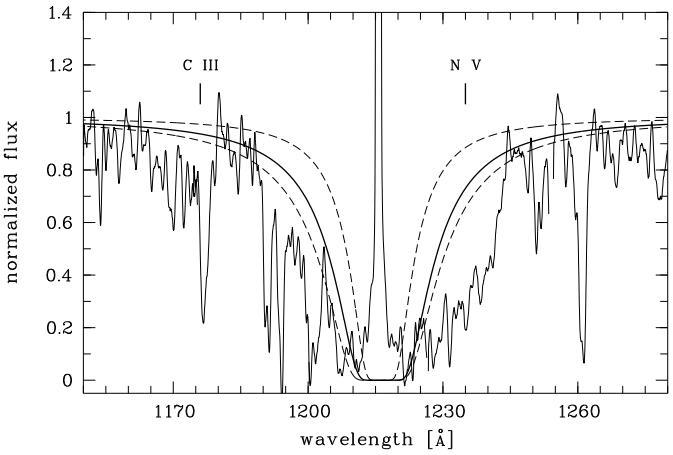

Fig. 2. The H I Ly α absorption, fitted by a Voigt profile (solid line) with contributions of $N(\mathrm{H\,I}) = 5.0 \times 10^{20}\,\mathrm{cm^{-2}}$ from galactic gas at $-15\,\mathrm{km\,s^{-1}}$ and $N(\mathrm{H\,I}) = 2.0 \times 10^{21}\,\mathrm{cm^{-2}}$ from LMC gas at $+255\,\mathrm{km\,s^{-1}}$. For comparison, the dashed lines show fits with H I column densities of 0.8 and $3.0 \times 10^{21}\,\mathrm{cm^{-2}}$ for the LMC component. Stellar absorption features in the damping wings of Ly α are identified above the spectrum. Geocoronal H I produces the strong emission in the centre of the absorption structure

2.8. Neutral Hydrogen

There are no accurate 21 cm data available for the sight-line to LH 10:3120, but the H I column density in this direction can be determined by fitting the damping wings of the strong Ly α absorption line in the *ORFEUS* spectrum. Obviously, the Ly α line (Fig. 2) is blended by the stellar N V line near 1240 Å and by some strong interstellar absorption lines near 1190 Å (e.g. Si II). In addition, the noise also disturbs the shape of the profile. No P Cygni profile is visible for the stellar N V, as seen in spectra of other early type stars. Since the right wing of the Ly α absorption is completely blended by the stellar N V line, we fit the left wing of Ly α with a theoretical Voigt profile, using oscillator strengths and damping parameters from the list of Morton (1991).

The H I absorption from galactic foreground gas in direction to the LMC is known to be $\sim 3 - 4 \times 10^{20}\,\mathrm{cm^{-2}}$ (McGee et al. 1983). Moreover, from the galactic S II abundance in our spectrum ($N(\mathrm{S\,II}) \leq 8.0 \times 10^{15}\,\mathrm{cm^{-2}}$) in combination with the known ratio $[\mathrm{S\,II/H}]_{\mathrm{MW}} = -4.8$ dex (de Boer et

[2] Galactic CO absorption is also visible in the weaker E-X band near 1076 Å, so that we conclude that the absorption structure at $-15\,\mathrm{km\,s^{-1}}$ in Fig. 1 doubtless is due to galactic CO absorption, too. The analysis of the molecular absorption lines related to Milky Way gas will be presented elsewhere

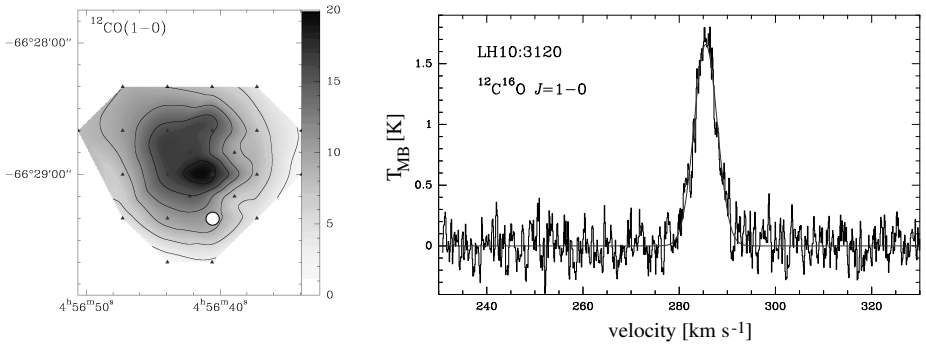

Fig. 3. Radio measurements of ^{12}CO are presented. *Left panel:* Contour map of ^{12}CO in the direction towards LH 10:3120 (marked with the open circle). The amount of CO increases to the North, where the geometrical centre of LH 10 is located. *Right panel:* The spectrum of ^{12}CO shows the maximum intensity near $+286\,\mathrm{km\,s^{-1}}$ (LSR)

al. 1987) we place un upper limit of $5.0 \times 10^{20}\,\mathrm{cm^{-2}}$ for galactic foreground absorption in H I in front of LH 10:3120. For the profile fit we fixed the galactic component ($-15\,\mathrm{km\,s^{-1}}$) at the latter column density and varied the LMC component at $+255\,\mathrm{km\,s^{-1}}$ in order to reproduce the observed absorption structure. We find the best agreement with a H I column density of $N(\mathrm{H\,I}) = 2.0 \times 10^{21}\,\mathrm{cm^{-2}}$ for the LMC gas, as shown in Fig. 2 (solid line). The uncertainty in this value is basically determined by the range of possible profile fits and not so much due to the uncertainty in the galactic foreground absorption. Varying the H I column density for the LMC component we find a reasonable agreement for profile fits in a range between 0.8 and 3.0 $\times 10^{21}\,\mathrm{cm^{-2}}$, in Fig. 2 shown as dashed lines.

2.9. Dust

For the determination of the gas-to-dust ratio as well as for the investigation of the relation between dust and molecular hydrogen the colour excess $E(B-V)$ *within* the LMC has to be estimated. Parker et al. (1992) give a minimum value of $E(B-V) = 0.17$ for the total reddening towards LH 10:3120. If we assume his value of $E(B-V) = 0.05$ as the galactic foreground reddening, 0.12 mag remains for the colour excess within the LMC. However, the galactic foreground reddening shows variations over the field of the LMC (Bessel 1990) of the order of $\Delta E(B-V) = 0.05$, so that the colour excess in the LMC toward LH 10:3120 is uncertain to the same degree.

One may consider that the selective extinction $R_V = A_V/E(B-V)$ in the LMC is different from that in the Galaxy. Research in the past has shown that the difference between $R_{V,\mathrm{LMC}}$ and $R_{V,\mathrm{MW}}$ is negligible with regard to the expected error for $E(B-V)_{\mathrm{LMC}}$ (Koornneef 1982; Cardelli et al. 1989). For the further discussion we will stick to the Galactic R_V-value. The problem of the re-normalization of $E(B-V)$ has been discussed in Mathis (1990; Sect. 2.1.1).

3. SEST measurements

3.1. Observations

The CO observations toward LH 10:3120 have been carried out in July 1997 using the 15-m Swedish-ESO Submillimetre Telescope (*SEST*) at La Silla, Chile. A SIS receiver at λ = 3 mm range was employed which yielded overall system temperatures, including sky noise, of order $T_{\mathrm{sys}} = 400\,\mathrm{K}$ on a main beam brightness temperature (T_{MB}) scale. The backend was an acousto-optical spectrometer (AOS) with 1000 contiguous channels and the channel separation of 43 kHz corresponds to $0.11\,\mathrm{km\,s^{-1}}$ at 115 GHz. The antenna beamwidth was 43″ at the observed line frequencies (Lovas 1992). The observations were carried out in a dual beam-switching mode (switching frequency 6 Hz) with a beam throw of 11′40″ in azimuth. All spectral intensities were converted to a T_{MB} scale, correcting for a main beam efficiency of 0.68 at 115 GHz. Calibration was checked by monitoring on Orion KL and M17SW and was found to be consistent between different observation periods within ± 10%. The pointing accuracy, obtained from measurements of the SiO masers R Dor, was better than 10″.

3.2. Results

Fig. 2 shows the results obtained with *SEST* in the direction of LH 10:3120. The presence of CO near LH 10 already had been shown by Cohen et al. (1988). The *SEST* contour map (Fig. 3, left panel) shows the presence of ^{12}CO emission over the whole measured area. The amount of CO increases to the north, where the (geometrical) centre of the young association LH 10 is located. The peak of the CO emission toward LH 10:3120 is near $V_{\mathrm{LSR}} = +286\,\mathrm{km\,s^{-1}}$ (Fig. 3, right panel). No CO is visible near $+255\,\mathrm{km\,s^{-1}}$, where the H_2 absorption has been found. Thus, the CO emission takes place at a radial velocity $30\,\mathrm{km\,s^{-1}}$ larger than where the H_2 cloud has its absorption (see Sect. 2.4). For the component at $+286\,\mathrm{km\,s^{-1}}$ we find a brightness temperature of $T_{\mathrm{MB}} = 1.66\,\mathrm{K}$. The velocity shift between CO emission and H_2 absorption as well as the lack of CO absorption at LMC velocities implies that the CO emission near $+286\,\mathrm{km\,s^{-1}}$ most likely comes from gas *behind* LH 10:3120. The *SEST* data therefore can not be used to compare the CO emission in the direction toward LH 10:3120 with the H_2 column density along this line of sight. Consequently, the determination of a X factor for the LMC gas is not possible.

4. Discussion

The main results of our measurements of the LMC gas towards LH 10:3120 have been compiled in Table 3. These results allow us to investigate the correlations between atomic gas, dust and molecules in the LMC.

Table 3. The LMC gas towards LH 10:3120

$N(\mathrm{H\,I})$	.....	$2.0 \times 10^{21}\,\mathrm{cm}^{-2}$
$N(\mathrm{H_2})$	.....	$6.6 \times 10^{18}\,\mathrm{cm}^{-2}$
$N(\mathrm{CO})$	.....	$\leq 3.3 \times 10^{13}\,\mathrm{cm}^{-2}$
$E(B-V)_{\mathrm{LMC}}$	.....	0.12
$N(\mathrm{H\,I})/E(B-V)_{\mathrm{LMC}}$ [a]	.....	$1.7 \times 10^{22}\,\mathrm{cm}^{-2}$
f	.....	0.007
$N(\mathrm{H_2})/N(\mathrm{CO})$	.....	$\geq 2.0 \times 10^{5}$

[a] mean galactic value: $4.8 \times 10^{21}\,\mathrm{cm}^{-2}$ (Bohlin et al. 1978)

Generally, the amount of molecular species is small in comparison with the total gas quantity. The hydrogen fraction in molecular form in the LMC is only $f = 2N(\mathrm{H_2})/[N(\mathrm{H\,I}) + 2N(\mathrm{H_2})] = 0.007$, lower than typical fractions for Milky Way gas with similar values in $N(\mathrm{H\,I})$ (Savage et al. 1977). Moreover, the upper limit for the CO column density in comparison to $N(\mathrm{H\,I})$ is, with regard to results for the Milky Way (Federman et al. 1980), relatively low as well. In contrast, the lower limit of $N(\mathrm{H_2})/N(\mathrm{CO})$ is 2.0×10^5 and thus not substantially different from ratios measured in the Galaxy. The excitation temperatures for the H_2 are 50 K for $J \leq 1$ and 470 K for $2 \leq J \leq 4$ (Paper I) and do not indicate an abnormally strong UV radiation field in the LMC gas towards LH 10:3120. A strong UV flux would decrease the molecular gas fraction through enhanced dissociation. We thus conclude that the diffuse LMC gas in the line of sight to LH 10:3120 initially has a lower molecule content than comparable gas in the Milky Way. Recently, low molecule fractions for LMC gas also have been proposed by Gunderson et al. (1998) for two other lines of sight to the LMC, using spectra at low dispersion from the *HUT* telescope. Moreover, the only FUV measurement of H_2 in the SMC so far shows a very low fraction of hydrogen in molecular form, too (Richter et al. 1998).

In searching for explanations for the low molecule fraction the lower dust content in the LMC gas, as reviewed by Koornneef (1984), might play a important role.

The gas-to-dust ratio in the LMC gas towards LH 10:3120 is with $N(\mathrm{H\,I})/E(B-V) = 1.7 \times 10^{22}\,\mathrm{cm}^{-2}$ about 4 times higher than the galactic value, while the ratios of $N(\mathrm{H_2})/E(B-V)$ and $N(\mathrm{CO})/E(B-V)$ are not significantly different compared to what we find in the Milky Way (see Savage et al. 1977; Federman et al. 1980). Clayton & Martin (1985) suggested that the ratio of $N(\mathrm{CNO})$ to $E(B-V)$ might be the same in the Milky Way and in the LMC, implying that the amount of dust and the abundance of gaseous CNO elements are decreased in the same degree. Does the lower dust content in the LMC (and SMC) also limit the amount of molecular hydrogen, at least in the diffuse ISM ?

Yet, the number of relevant observations is too low to draw meaningful conclusions about the molecular content in the overall diffuse ISM of the Magellanic Clouds. Nevertheless, all measurements made so far and discussed here support the scenario, in which the amount of H_2 in the diffuse ISM of the Magellanic Clouds is limited by the lower dust abundance. Clearly, the lower metallicity of the Magellanic Clouds leads to a smaller dust amount as well as to a reduced abundance of CO, so that the lower dust content probably allows (in the mean) less H_2 to form. Due to the deficiency of dust the shielding from the UV radiation is reduced, too. Therefore, the total abundance of H_2 in the diffuse ISM compared to the amount of neutral hydrogen is probably lower than in the Milky Way. The intrinsic ratio of H_2 to CO in the diffuse gas of a metal-poor galaxy like the Magellanic Clouds might not be different at all from the one in the Milky Way, since it is possible that the abundance of both H_2 and CO is reduced by a similar factor.

For the densest regions in the interstellar gas, the molecular clouds, the H_2/CO ratio is an even more critical parameter, since we do not know how different the cloud sizes in H_2 and CO in a low metallicity environment really are. Pak et al. (1998) argued that the lower abundances of carbon and oxygen in the Magellanic Clouds may result in signifcantly lower cloud sizes as observed in CO emission compared to the size in molecular hydrogen. Hence we might underestimate the total mass of a molecular cloud when obtaining the H_2 amount in a metal-deficient galaxy using a standard conversion factor between H_2 column density and CO luminosity (Maloney & Black 1988). We can not measure the H_2/CO ratio *within* the cloud cores. Thus, it is important to find its value at least in the more diffuse cloud envelopes. We then will be able to estimate how certain the usage of a conversion between CO luminosity and H_2 column density in a galaxy with a low metallicity can be at all.

Future UV satellites, such as *FUSE*, will help to study the relations between atomic and molecular gas in the Magellanic Clouds and other galaxies in more detail. Only good statistics of sight-line measurements in these systems will allow a meaningful comparison between gas properties in metal-deficient galaxies and the Milky Way.

Acknowledgements. We thank John Black for helpful comments and the Heidelberg-Tübingen team for their great support. PR is supported by a grant from the DARA (now DLR) under code 50 QV 9701 3. YNC thanks the National Science Council of Taiwan for its financial support through grant 86-2112-M001-032.

References

Appenzeller I., Krautter J., Mandel H., Oestreicher R., 1988, In: A decade of UV astronomy with *IUE*. ESA SP-281, 2, 337
Barnstedt J., Kappelmann N., Appenzeller I., et al., 1999, A&AS 134, 561
Bessel M.S., 1990, A&A 242, L17
Bloemen J.B.G.M., Strong A.W., Blitz L., et al., 1986, A&A 154, 25
Bohlin R.C., Savage B.D., Drake J.F., 1978, ApJ 224, 132
Cardelli J.A., Clayton G.C., Mathis J.S., 1989, ApJ 345, 245
Chin Y.-N., Henkel C., Whiteoak J.B., et al., 1997, A&A 317, 548
Chin Y.-N., Henkel C., Millar T.J., et al., 1998, A&A 330, 901
Clayton G., Martin P.G., 1985, ApJ 288, 558
Cohen R.S., Dame T.M., Garay G., et al., 1988, ApJ 331, L95
de Boer K.S., Jura M.A., Shull J.M., 1987, In: Kondo Y., et al. (eds.) Exploring the Universe at Ultraviolet Wavelengths. Reidel, Dordrecht, p. 485
de Boer K.S., Richter P., Bomans D.J., Heithausen A., Koornneef J., 1998, A&A 338, L5 (Paper I)

Federman S.R., Glassgold A.E., Jenkins E.B., Shaya E.J., 1980, ApJ 242, 545
Fligge M., Solanki S.K., 1997, A&AS 124, 579
Gunderson K.S., Clayton G.C., Green J.C., 1998, PASP 110, 60
Heithausen A., Mebold U., 1989, A&A 214, 347
Israel F.P., 1997, A&A 328, 471
Jenkins E.B., Drake J.F., Morton D.C., et al., 1973, ApJ 181, L122
Koornneef J., 1982, A&A 107, 247
Koornneef J., 1984, In: van den Bergh S., de Boer K.S. (eds.) IAU Symp.108, Structure and Evolution of the Magellanic Clouds. Reidel, Dordrecht, p. 333
Lovas F.J., 1992, J. Phys. Chem. Ref. Data 21, 181
Maloney P., Black J., 1988, ApJ 325, 389
Mathis J.S., 1990, ARA&A 28, 37
McGee R.X., Newton L.M., Morton D.C., 1983, MNRAS 205, 1191
Morton D.C., 1991, ApJS 77, 119
Morton D.C., Dinerstein H.L., 1976, ApJ 204, 1
Morton D.C., Noreau L., 1994, ApJS 95, 301
Pak S., Jaffe D.T., van Dishoeck E.F., Johansson L.E.B., Booth R.S., 1998, ApJ 498, 735
Parker J.W., Garmany C.D., Massey P., Walborn N.R., 1992, AJ 103, 1205
Richter P., Widmann H., de Boer K.S., et al., 1998, A&A 338, L9
Rubio M., Lequeux J., Boulanger F., et al., 1993, A&A 271, 1
Savage B.D., Bohlin R.C., Drake J.F., Budich W., 1977, ApJ 216, 291